NANO LETTERS

Letter

pubs.acs.org/NanoLett

Scalable Synthesis of Uniform Few-Layer Hexagonal Boron Nitride Dielectric Films

P. Sutter,*,† J. Lahiri,† P. Zahl,† B. Wang,‡ and E. Sutter†

†Center for Functional Nanomaterials, Brookhaven National Laboratory, Upton, New York 11973, United States

‡Department of Physics & Astronomy, Vanderbilt University, Nashville, Tennessee 37235, United States

Supporting Information

ABSTRACT: Two-dimensional or ultrathin layered materials are attracting broad interest in both fundamental science and applications. While exfoliation can provide high-quality single- and few-layer flakes with nanometer to micrometer size, the development of wafer-scale synthesis methods is important for realizing the full potential of ultrathin layered materials. Here we demonstrate the growth of high quality few-layer boron nitride (BN) films with controlled thickness by magnetron sputtering of B in N_2/Ar, a scalable process using only benign, nontoxic reagents. BN films up to two atomic layers are synthesized by reactive deposition at high substrate temperatures. Thicker monocrystalline BN films with an arbitrary number of atomic layers are achieved in a two-step process comprising cycles of alternating room temperature deposition and annealing. Tunneling transport across these BN films shows pinhole-free insulating behavior on μm^2 scales, demonstrating the realization of high quality ultrathin dielectrics.

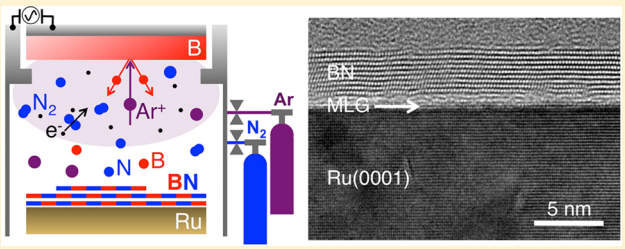

KEYWORDS: *Layered materials, boron nitride, ultrathin dielectric films, thin film growth, reactive magnetron sputtering, tunneling*

Graphene, an atomically thin sheet of sp^2 bonded carbon, has attracted broad research interest, and its extreme properties promise to enable a wide range of future applications.[1,2] Among other two-dimensional or ultrathin layered materials,[3] boron nitride (BN) appears particularly well suited for integration with graphene, for instance as a gate dielectric for high-mobility field effect devices[4] or for designing novel layered heterostructures.[5] The two materials are isoelectronic and isostructural with minimal (~1.6%) lattice mismatch,[6] yet have different band structures (semimetallic and insulating, respectively) giving rise to complementary (opto-) electronic characteristics.

Mechanical[3] or liquid-phase[7] exfoliation provide high-quality single- and few-layer flakes of materials such as graphene and BN. However, the broader exploration of new phenomena and applications depends critically on the development of scalable synthesis methods for ultrathin layered materials. Chemical vapor deposition (CVD)[8,9] and carbon segregation[10] on transition metals are now among the primary methods for graphene synthesis. CVD methods have also been used for the growth of BN[11,12] and hybrid graphene−BN monolayers,[13,14] and recent reports raised the possibility that such methods might be extended to the growth of few-layer BN.[15,16] BN films with controlled thickness prepared by solution methods[17] show promise for applications in nanocomposites,[18] but it remains unclear if solution synthesis or vapor chemical routes with engineered precursors[19] can yield high-quality BN at wafer scales. No approach has yet provided crystalline BN films with uniform thickness in the range between 2 and 20 BN layers, crucial to applications as ultrathin dielectrics in novel device schemes in conjunction with graphene, such as bistable field-effect transistors (BisFETs)[20,21] or tunneling devices.[5]

Physical vapor deposition could avoid the complex set of interrelated growth parameters governing CVD processes. While commonly associated with polycrystalline thin films, for example, in metallurgical coatings or transparent conducting oxides, magnetron sputtering has been used to grow epitaxial metals,[22,23] compounds,[24] and semiconductor heterostructures,[25] including high electron mobility modulation-doped quantum wells.[26] Here we demonstrate the growth of high quality few-layer BN films with controlled thickness using reactive magnetron sputtering of B in N_2/Ar, a scalable, industry-compatible process that uses only benign, nontoxic reagents.

The glow discharge of the magnetron sputtering process plays two important roles in the growth of BN films (Figure 1 a):[27,28] (i) evaporation of B by collision cascades due to the impact of energetic Ar^+ ions on a solid B target; and (ii) generation of nitrogen radicals via dissociation of gas phase N_2 by free electrons and ions in the plasma. On an appropriate substrate (here epitaxial Ru(0001) thin films) heated to high temperature, B and N species assemble into a well-ordered film consisting of layered atomic h-BN sheets (Figure 1b). Optimum growth conditions produce crystalline stacks of BN sheets with low thickness variation (±1 layer) across the entire sample and consistent [B]/[N] atomic ratios of (1.0 ± 0.05),

Received: November 5, 2012
Revised: December 10, 2012
Published: December 17, 2012

 © 2012 American Chemical Society

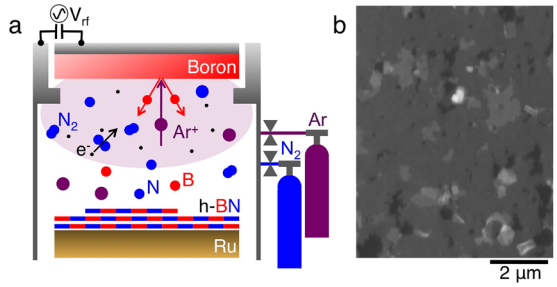

Figure 1. Hexagonal boron nitride growth by reactive magnetron sputtering. (a) Schematic diagram of the planar magnetron geometry for deposition from a solid boron target in Ar/N_2 gas. (b) UHV scanning electron micrograph of the surface of a three-layer h-BN film on epitaxial $Ru(0001)/Al_2O_3$. The secondary electron intensity scales with the BN thickness.

determined from the intensities of B1s and N1s core levels in X-ray photoelectron spectroscopy (XPS; Supporting Information, Figure S1).

Apart from the equilibrium h-BN phase, thin film deposition at temperatures far below those used for growing BN single crystals[29] can give rise to well-ordered metastable crystalline phases, such as rhombohedral BN (rBN), a BN polymorph in which honeycomb atomic BN layers are arranged in non-equilibrium A−B−C stacking order.[30] In BN growth by magnetron sputtering on Ru, the termination of the metal surface determines the layer stacking and hence the BN phase that forms. Whereas direct growth onto clean Ru(0001) produces h-BN (A−A′−A stacking; Figure 2), the termination

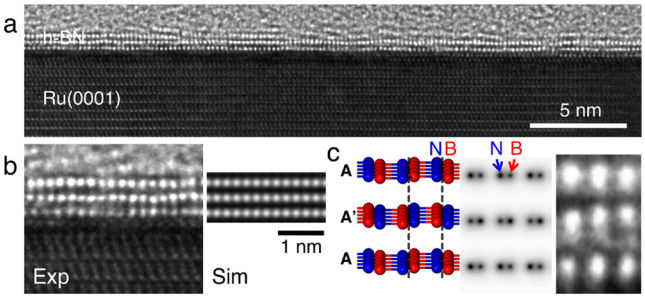

Figure 2. A−A′−A stacked h-BN on Ru(0001). (a) Overview HRTEM image of a three-layer BN film. (b) Comparison of the experimental contrast with a dynamic image simulation assuming the equilibrium A−A′−A stacking of h-BN. (c) Model of A−A′−A stacked h-BN, computed electron density map, and experimental HRTEM image.

of the Ru surface with a graphene monolayer prior to BN growth induces a different stacking order (A−B−C; Figure 3), that is, produces rBN. Monolayers of both graphene and boron nitride on Ru(0001) have complex moiré structures, either a BN nanomesh[12] for BN growth directly onto Ru(0001) (Figure S2 of the Supporting Information), or a graphene moiré[31] with inhomogeneous charge distribution in the two C sublattices.[32] Calculations show rBN and conventionally stacked h-BN nearly degenerate in the bulk,[33] but our results suggest that different interface configurations favor different incipient stacking sequences (A−A′ or A−B) defined by the first BN sheet beyond the interfacial layer, which then persist for the entire thickness of the BN film (Figure 3). While A−A′−A stacked h-BN and A−B−C stacked rBN have very similar electronic structures,[33] that is, they likely show comparable dielectric

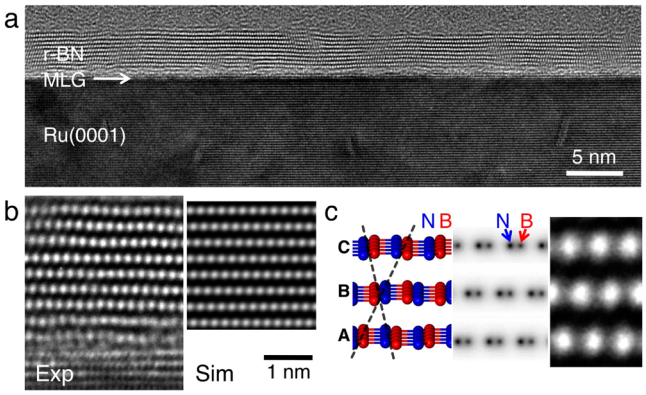

Figure 3. A−B−C stacked rhombohedral BN on graphene-covered Ru(0001). (a) Overview HRTEM image of a 10-layer BN film. (b) Comparison of the experimental contrast with a dynamic image simulation assuming nonequilibrium A−B−C stacking. (c) Model of A−B−C stacked (rhombohedral) BN, computed electron density map, and experimental HRTEM image.

properties, control over the stacking sequence can add significantly to the tools for BN materials processing. For example, the kinetics of conversion of the two hexagonal BN phases to cubic (zincblende) c-BN should be very different, with rBN transforming along a facile, diffusionless pathway.[33,34] Thus, the selective growth of single crystalline rBN could provide a basis for the formation of ultrathin, high-quality cubic BN films.

The realization of ordered films with controlled thickness is an important requirement for a rational BN synthesis method. The preparation of uniform single monolayer BN on metals has been facilitated by the low chemical reactivity of the h-BN surface, which leads to a self-termination of growth by low-pressure borazine CVD after the completion of a monolayer film (Figure 4i).[35,36] The synthesis of few-layer BN films with uniform thickness is significantly more challenging and has not been achieved by CVD. We have identified different growth scenarios in reactive magnetron sputtering that provide high-quality BN films with good thickness uniformity. Via deposition at high substrate temperatures (850−900 °C), crystalline films up to two layers thickness are obtained. Analysis by XPS shows a progressive reduction of the growth rate such that two complete BN layers are only achieved asymptotically (Figure 4ii). The slowing of the growth rate and apparent inability to realize films with more than two layers using slow deposition at high substrate temperature is consistent with a thickness-dependent sticking coefficient of the deposited B/N species on the BN surface. The first BN layer is readily achieved due to the high reactivity and sticking coefficient of the metal surface. The observed saturation coincides with the transition from a still moderately reactive, corrugated interfacial BN layer[37] to a BN bilayer with much lower surface reactivity approaching that of bulk BN. The drop in reactivity at a thickness of 2 BN layers is corroborated by ab initio calculations of the projected density of states (DOS; Figure S3), and of the binding energy of a B_3N_3 radical used to model adsorption on the BN surface. Monolayer BN on Ru shows a finite DOS near the Fermi level (E_F) and a high binding energy of B_3N_3 (0.9 eV). For bilayer BN on Ru, a large bandgap comparable to that of bulk BN opens up. The DOS at E_F is negligible, and the computed B_3N_3 binding energy (0.5 eV) becomes equal to that on bulk BN (see Supporting

dx.doi.org/10.1021/nl304080y | Nano Lett. 2013, 13, 276−281

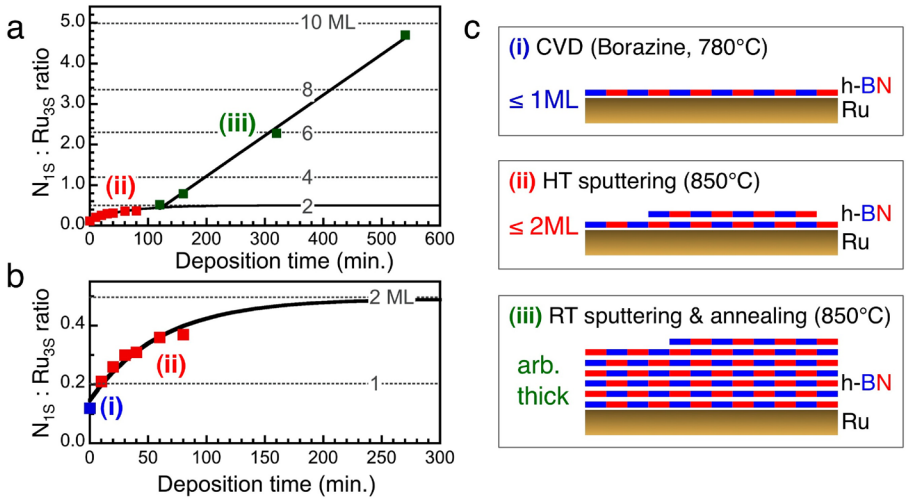

Figure 4. Regimes of few-layer h-BN growth by chemical vapor deposition and reactive magnetron sputtering. (a, b) XPS analysis of the N1s to Ru3s core level intensity ratio for growth by: (i) low-pressure CVD using borazine (780 °C); (ii) reactive magnetron sputtering at high temperature (850 °C); (iii) alternating room temperature sputtering and annealing to 850 °C. (c) Schematic representation of the thickness regimes accessible by the different h-BN growth methods.

Information); that is, adsorption of B/N species and BN nucleation beyond two layers are suppressed.

The two-layer limit can be overcome by an alternative growth scenario (Figure 4iii). Reactive sputtering onto substrates held at room temperature involves a constant, thickness-independent BN deposition rate close to the initial rate observed for high temperature growth, consistent with a high sticking coefficient of the deposited species. Room-temperature deposition produces amorphous or nanocrystalline BN films, whose N1s and B1s XPS spectra are dominated by peaks that are red-shifted (by 0.71 and 0.79 eV, respectively) compared to those of well-ordered, monocrystalline BN synthesized at high temperature (Figures S4 and S5). Thin nanocrystalline BN films are recrystallized by vacuum annealing to 850 °C, which eliminates the red-shifted XPS lines and transfers the entire spectral weight into the characteristic peaks of well-ordered, crystalline h-BN. Via alternating deposition of the equivalent of ~1 BN atomic layer in nanocrystalline form and crystallization at high temperature, layered h-BN films with controlled thickness and good uniformity (±1 layer) are realized on epitaxial Ru(0001)/Al_2O_3 substrates (Figures 2−4). Use of a thin nanocrystalline precursor layer ensures that only short-range mass transport and rebonding are required to form a new h-BN sheet, whereas the already completed layers act as an inert support. The stoichiometric [B]/[N] ratio, that is, absence of any detectable N loss, suggests that the deposited B−N species remain intact while becoming part of the growing crystalline sheet during annealing. This overall scenario is similar to the annealing of polyborazylene on Ni,[16] which results in crystalline h-BN but has not shown atomic-layer thickness control.

Ultrahigh vacuum scanning electron microscopy on thicker BN films shows a well-ordered surface consisting of μm-sized terraces with uniform height delineated by sharp steps, consistent with the expected appearance of atomic layers in crystalline h-BN (Figure S6). Raman spectroscopy on annealed films detects a narrow line due to the E_{2g} zone center mode at 1362 cm^{-1} (Figure S7a). The optical properties of few-layer BN films on Ru(0001) have been investigated by UV−visible absorption spectroscopy (Figure S7b,c). A 10-layer BN film shows low absorbance in the near-infrared and visible spectral range and a sharp increase in absorption at UV wavelengths (Figure S7b), as expected for a large-bandgap dielectric. Analysis of the UV absorption (Figure S7c) yields a direct optical bandgap of (5.85 ± 0.05) eV, in good agreement with measurements on thicker crystalline BN layers[16] and BN single crystals.[38]

To evaluate the dielectric properties of our few-layer h-BN films, we have fabricated test structures in which the active BN layer is sandwiched between the Ru(0001) substrate and thin, circular Ru top electrodes defined by shadow mask deposition in UHV (Figure 5a). Individual device structures were addressed via three-axis nanomanipulated probe tips for vertical transport measurements (Figure 5b,c). The results of representative measurements are summarized in Figure 5d,e.

Tunneling current−voltage (I−V) characteristics consistently show a small, linearly increasing current at low bias, followed by a transition to an exponential rise in current signaling the onset of dielectric breakdown in the BN film in the high-bias regime (Figure 5d). Similar to graphene,[39] exfoliation of BN from bulk crystals or powders provides few-layer material with very low defect density that can serve as a benchmark for the quality of bottom-up synthesized BN films. Comparing the I−V characteristics of micrometer-scale structures of six-layer BN (grown by alternating room temperature deposition and annealing; Figure 4iii) sandwiched between Ru electrodes with recent measurements within small diameter (25 nm) contact areas on exfoliated BN,[40] we find low-bias tunneling conductances consistent with direct tunneling through (6 ± 1) atomic layers of h-BN (Figure 5e), that is, pinhole-free, uniform dielectric behavior over the ~3 μm^2 active areas of our devices.

Previous work on BN growth on metal foils (Cu,[41−44] Ni[16]) has stressed the need to isolate the films and transfer them to other supports for possible use in devices, such as UV light emitters.[38,45] High-quality few-layer BN on epitaxial metal thin films offer the alternative possibility of a bottom-up assembly of an entire device structure—comprising an insulating substrate, metallic gate contact and BN dielectric—and ultimately the active channel of a graphene field-effect device—without any metal etching or layer transfers. Our approach to the synthesis

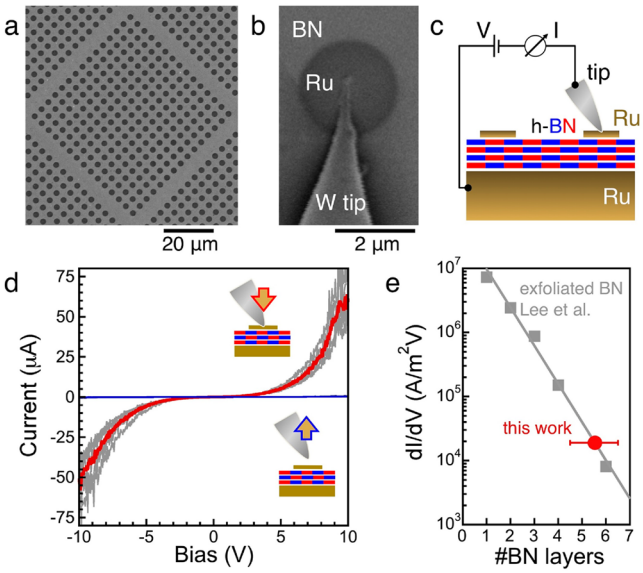

Figure 5. Vertical transport through six-layer h-BN sandwiched between Ru electrodes. (a) UHV SEM image of a Ru top electrode pattern fabricated in situ by shadow mask deposition of Ru onto six-layer h-BN/Ru(0001). (b) UHV SEM image of one of the Ru electrodes (2 μm diameter) contacted by a W probe tip. (c) Schematic of the vertical transport measurement on h-BN between Ru electrodes. (d) Current−voltage characteristics measured with W probe tunneling above (blue) and in contact with (red) the top Ru electrode. Red trace: average over 10 individual measurements, shown as gray lines. (e) Comparison of the specific tunneling conductance of a BN/Ru(0001) film grown by reactive magnetron sputtering (six layers thick) with that of exfoliated BN (Lee et al.[40]), normalized to the device area.

of few-layer BN films with good thickness uniformity provides an avenue for realizing this vision, and represents an important step toward developing the bottom-up synthesis of graphene-BN hybrid layered materials. Future work can extend our method to the growth of graphene layers on BN, thus setting the stage for the fabrication of devices and engineered heterostructures comprising alternating graphene and BN layers with controlled thickness.

Methods. BN films were grown in an ultrahigh-vacuum (UHV) system (base pressure 2×10^{-10} Torr) by reactive radio frequency (rf) magnetron sputtering (10 W rf power) of a boron target (2" dia., 99.5%, K.J. Lesker) in high-purity Ar/N_2 gas mixtures (20% N_2) with a total pressure of 10^{-2} Torr. Single crystalline, epitaxial Ru films (100 nm thick) on α-Al_2O_3(0001) (c-plane sapphire), deposited in situ, were used as substrates. In situ deposition of these Ru templates in the same UHV system in which the BN was grown, along with a negligible solubility of carbon in epitaxial Ru thin films,[46] ensured a high purity substrate and specifically helped avoid C incorporation in the BN films. A high-temperature heater allowed reaching substrate temperatures between room temperature and 1000 °C, measured by an IR pyrometer. Single-step growth (up to two BN layers) employed reactive magnetron sputtering at 850 °C substrate temperature. Cyclic growth (thicker BN films) used room temperature deposition (40 min) alternating with annealing at 850 °C (30 min). The BN films were characterized in situ by X-ray photoelectron spectroscopy (XPS) using Al Kα radiation and by room temperature scanning tunneling microscopy (STM). Ex situ analysis was performed by transmission electron microscopy (TEM) of cross sections of the films in a FEI Titan 80-300 microscope equipped with a CEOS Cs-corrector at 300 keV electron energy. Thin sections for TEM were prepared by focused ion beam milling. High-resolution TEM contrast simulations were carried out using the multislice method, as implemented in the software package JEMS.[47] Further characterization was performed by UHV scanning electron microscopy (Zeiss Gemini), tapping mode atomic force microscopy (Veeco Nanoscope V), and Raman spectroscopy (WiTec Alpha 300) using 532 nm excitation, a 100× objective (spot size 400 nm), and incident power below 1 mW. UV−visible spectroscopy has been measured in an integrating sphere reflection geometry using a Perkin-Elmer Lambda 950 UV−vis/NIR spectrophotometer. The optical bandgap, E_g, was determined from the photon-energy dependent absorption coefficient $\alpha(E)$ using the relation $(\alpha \cdot E)^2 = C(E - E_g)$ for a direct-gap material.[48]

The thickness and composition of the BN films were determined from XPS measurements by analyzing the intensities of Ru3s/N1s and N1s/B1s peaks, respectively. The thickness analysis took into account the different photoemission cross sections (Scofield factors) at $h\nu$ = 1486 eV, as well as the inelastic mean free paths of the Ru3s and N1s photoelectrons. In the analysis of the h-BN composition, the difference in mean free paths for N1s and B1s photoelectrons amounted to intensity differences below 2% for our thickest films (~10 BN layers) and was therefore neglected.

Test structures for tunneling transport experiments were fabricated by thermal evaporation of arrays of Ru disk electrodes (2 μm diameter, 5 nm thick) in UHV onto well-degassed BN/Ru(0001) thin films, using SiN shadow masks (50 nm thick, 2 μm openings; TEMwindows SN100-MP2Q05) aligned using a Nanostencil shadow mask lithography system.[49] Samples with Ru-BN-Ru sandwich structures were transferred in situ to a UHV nanomanipulation system for electrical transport measurements (Omicron UHV Nanoprobe). The bottom contact was made to the Ru thin film of the substrate, whereas the top Ru disk electrodes were contacted by using electrochemically sharpened W tips. The tip approach was accomplished using a tunneling (STM) feedback loop, and mechanical contact to the Ru electrodes then established by decreasing the tip−sample distance (viewed by field-emission SEM) until stable, reproducible current−voltage characteristics were obtained. Current−voltage curves were measured with the sample held at room temperature, using a programmable semiconductor test system (Keithley, model 4200SCS).

■ ASSOCIATED CONTENT

Supporting Information

Supplementary Figures S1−S7; computational methods (reactivity of BN surfaces); supplementary references. This material is available free of charge via the Internet at http://pubs.acs.org.

■ AUTHOR INFORMATION

Corresponding Author

*E-mail: psutter@bnl.gov.

Notes

The authors declare no competing financial interest.

■ ACKNOWLEDGMENTS

This research has been carried out at the Center for Functional Nanomaterials, Brookhaven National Laboratory, which is supported by the U.S. Department of Energy, Office of Basic Energy Sciences, under Contract No. DE-AC02-98CH10886. The authors thank Kim Kisslinger for technical support, and Dmytro Nykypanchuk for measuring UV−vis spectra.

■ REFERENCES

(1) Geim, A. K. Graphene: Status and Prospects. *Science* **2009**, *324*, 1530−1534.
(2) Castro Neto, A. H.; Guinea, F.; Peres, N. M. R.; Novoselov, K. S.; Geim, A. K. The electronic properties of graphene. *Rev. Mod. Phys.* **2009**, *81*, 109.
(3) Novoselov, K. S.; et al. Two-dimensional atomic crystals. *Proc. Natl. Acad. Sci. U.S.A.* **2005**, *102*, 10451−10453.
(4) Dean, C. R.; et al. Boron nitride substrates for high-quality graphene electronics. *Nat. Nanotechnol.* **2010**, *5*, 722−726.
(5) Britnell, L.; et al. Field-Effect Tunneling Transistor Based on Vertical Graphene Heterostructures. *Science* **2012**, *335*, 947−950.
(6) *New Semiconductor Materials. Characteristics and Properties.* http://www.ioffe.ru/SVA/NSM/Semicond/BN/ (accessed October 1, 2012).
(7) Coleman, J. N.; et al. Two-Dimensional Nanosheets Produced by Liquid Exfoliation of Layered Materials. *Science* **2011**, *331*, 568−571.
(8) Reina, A.; et al. Large Area, Few-Layer Graphene Films on Arbitrary Substrates by Chemical Vapor Deposition. *Nano Lett.* **2009**, *9*, 30−35.
(9) Li, X.; et al. Large-Area Synthesis of High-Quality and Uniform Graphene Films on Copper Foils. *Science* **2009**, *324*, 1312−1314.
(10) Sutter, P. W.; Flege, J.-I.; Sutter, E. A. Epitaxial graphene on ruthenium. *Nat. Mater.* **2008**, *7*, 406−411.
(11) Oshima, C.; Nagashima, A. Ultra-thin epitaxial films of graphite and hexagonal boron nitride on solid surfaces. *J. Phys: Condens. Matter* **1997**, *9*, 1.
(12) Corso, M.; et al. Boron Nitride Nanomesh. *Science* **2004**, *303*, 217−220.
(13) Sutter, P.; Cortes, R.; Lahiri, J.; Sutter, E. Interface Formation in Monolayer Graphene-Boron Nitride Heterostructures. *Nano Lett.* **2012**, *12*, 4869−4874.
(14) Levendorf, M. P.; et al. Graphene and boron nitride lateral heterostructures for atomically thin circuitry. *Nature* **2012**, *488*, 627−632.
(15) Song, L.; et al. Large Scale Growth and Characterization of Atomic Hexagonal Boron Nitride Layers. *Nano Lett.* **2010**, *10*, 3209−3215.
(16) Shi, Y.; et al. Synthesis of Few-Layer Hexagonal Boron Nitride Thin Film by Chemical Vapor Deposition. *Nano Lett.* **2010**, *10*, 4134−4139.
(17) Nag, A.; et al. Graphene Analogues of BN: Novel Synthesis and Properties. *ACS Nano* **2010**, *4*, 1539−1544.
(18) Kiran, M. S. R. N.; Raidongia, K.; Ramamurty, U.; Rao, C. N. R. Improved mechanical properties of polymer nanocomposites incorporating graphene-like BN: Dependence on the number of BN layers. *Scr. Mater.* **2011**, *64*, 592−595.
(19) Müller, F.; Hüfner, S.; Sachdev, H.; Gsell, S.; Schreck, M. Epitaxial growth of hexagonal boron nitride monolayers by a three-step boration-oxidation-nitration process. *Phys. Rev. B* **2010**, *82*, 075405.
(20) Min, H.; Bistritzer, R.; Su, J.-J.; MacDonald, A. H. Room-temperature superfluidity in graphene bilayers. *Phys. Rev. B* **2008**, *78*, 121401.
(21) Banerjee, S. K.; Register, L. F.; Tutuc, E.; Reddy, D.; MacDonald, A. H. Bilayer PseudoSpin Field-Effect Transistor (BiSFET): A Proposed New Logic Device. *IEEE Electron. Device Lett.* **2009**, *30*, 158−160.
(22) Sutter, P. W.; Albrecht, P. M.; Sutter, E. A. Graphene growth on epitaxial Ru thin films on sapphire. *Appl. Phys. Lett.* **2010**, *97*, 213101.
(23) Jiang, H.; Klemmer, T. J.; Barnard, J. A.; Payzant, E. A. Epitaxial growth of Cu on Si by magnetron sputtering. *J. Vac. Sci. Technol., A* **1998**, *16*, 3376−3383.
(24) Adibi, F.; et al. Defect structure and phase transitions in epitaxial metastable cubic Ti0.5Al0.5N alloys grown on MgO(001) by ultra-high-vacuum magnetron sputter deposition. *J. Appl. Phys.* **1991**, *69*, 6437−6450.
(25) Sutter, P.; et al. Magnetron sputter epitaxy of Si_mGe_n/Si(001) strained-layer superlattices. *Appl. Phys. Lett.* **1994**, *65*, 2220−2222.
(26) Sutter, P.; Groten, D.; Muller, E.; Lenz, M.; von Kanel, H. Quantum transport in sputtered, epitaxial Si/$Si_{1-x}Ge_x$ heterostructures. *Appl. Phys. Lett.* **1995**, *67*, 3954−3956.
(27) Berg, S.; Nyberg, T. Fundamental understanding and modeling of reactive sputtering processes. *Thin Solid Films* **2005**, *476*, 215−230.
(28) Jensen, H.; Jensen, U. M.; Sorensen, G. Deposition of boron-nitride films by nitrogen sputtering from a boron-metal target. *Appl. Phys. Lett.* **1995**, *66*, 1489−1491.
(29) Watanabe, K.; Taniguchi, T.; Kanda, H. Direct-bandgap properties and evidence for ultraviolet lasing of hexagonal boron nitride single crystal. *Nat. Mater.* **2004**, *3*, 404−409.
(30) Sato, T. Influence of Monovalent Anions on the Formation of Rhombohedral Boron Nitride, rBN. *Proc. Jpn. Acad.* **1985**, *61*, 459−463.
(31) Sutter, E. A.; Acharya, D. P.; Sadowski, J. T.; Sutter, P. W. Scanning tunneling microscopy on epitaxial bilayer graphene on ruthenium (0001). *Appl. Phys. Lett.* **2009**, *94*, 133101.
(32) Wang, B.; Bocquet, M.-L.; Marchini, S.; Günther, S.; Wintterlin, J. Chemical origin of a graphene moire overlayer on Ru(0001). *Phys. Chem. Chem. Phys.* **2008**, *10*, 3530−3534.
(33) Furthmüller, J.; Hafner, J.; Kresse, G. Ab initio calculation of the structural and electronic properties of carbon and boron nitride using ultrasoft pseudopotentials. *Phys. Rev. B* **1994**, *50*, 15606−15622.
(34) Medlin, D. L.; Friedmann, T. A.; Mirkarimi, P. B.; Mills, M. J.; McCarty, K. F. Evidence for rhombohedral boron nitride in cubic boron nitride films grown by ion-assisted deposition. *Phys. Rev. B* **1994**, *50*, 7884−7887.
(35) Paffettt, M. T.; Simonson, R. J.; Papin, P.; Paine, R. T. Borazine Adsorption and Decomposition at Pt(111) and Ru(001) Surfaces. *Surf. Sci.* **1990**, *232*, 286−296.
(36) Sutter, P.; Lahiri, J.; Albrecht, P.; Sutter, E. Chemical Vapor Deposition and Etching of High-Quality Monolayer Hexagonal Boron Nitride Films. *ACS Nano* **2011**, *5*, 7303−7309.
(37) Berner, S.; et al. Boron Nitride Nanomesh: Functionality from a Corrugated Monolayer. *Angew. Chem.* **2007**, *119*, 5207−5211.
(38) Watanabe, K.; Taniguchi, T.; Niiyama, T.; Miya, K.; Taniguchi, M. Far-ultraviolet plane-emission handheld device based on hexagonal boron nitride. *Nat. Photonics* **2009**, *3*, 591−594.
(39) Morozov, S. V.; et al. Giant intrinsic carrier mobilities in graphene and its bilayer. *Phys. Rev. Lett.* **2008**, *100*, 016602.
(40) Lee, G.-H.; et al. Electron tunneling through atomically flat and ultrathin hexagonal boron nitride. *Appl. Phys. Lett.* **2011**, *99*, 243114−243113.
(41) Ci, L.; et al. Atomic layers of hybridized boron nitride and graphene domains. *Nat. Mater.* **2010**, *9*, 430−435.
(42) Liu, Z.; et al. Direct Growth of Graphene/Hexagonal Boron Nitride Stacked Layers. *Nano Lett.* **2011**, *11*, 2032−2037.
(43) Kim, K. K.; et al. Synthesis of Monolayer Hexagonal Boron Nitride on Cu Foil Using Chemical Vapor Deposition. *Nano Lett.* **2011**, *12*, 161−166.
(44) Lee, K. H.; et al. Large-Scale Synthesis of High-Quality Hexagonal Boron Nitride Nanosheets for Large-Area Graphene Electronics. *Nano Lett.* **2012**, *12*, 714−718.
(45) Kubota, Y.; Watanabe, K.; Tsuda, O.; Taniguchi, T. Deep Ultraviolet Light-Emitting Hexagonal Boron Nitride Synthesized at Atmospheric Pressure. *Science* **2007**, *317*, 932−934.
(46) Sutter, P.; Ciobanu, C. V.; Sutter, E. Real-Time Microscopy of Graphene Growth on Epitaxial Metal Films: Role of Template Thickness and Strain. *Small* **2012**, *8*, 2250.

(47) Stadelmann, P. A. JEMS-EMS Java Version. http://cimewww.epfl.ch/people/stadelmann/jemsWebSite/jems.html (accessed August 15, 2012).
(48) Tauc, J. Optical properties and electronic structure of amorphous Ge and Si. *Mater. Res. Bull.* **1968**, *3*, 37−46.
(49) Zahl, P.; Bammerlin, M.; Meyer, G.; Schlittler, R. R. All-in-one static and dynamic nanostencil atomic force microscopy/scanning tunneling microscopy system. *Rev. Sci. Instrum.* **2005**, *76*, 023707−023705.

Supplementary Online Material

Scalable Synthesis of Uniform Few-Layer Hexagonal Boron Nitride Dielectric Films

P. Sutter,[1] J. Lahiri,[1] P. Zahl,[1] B. Wang,[2] and E. Sutter[1]

[1]*Center for Functional Nanomaterials, Brookhaven National Laboratory, Upton, New York 11973 (USA)*

[2]*Department of Physics & Astronomy, Vanderbilt University, Nashville, TN 37235*

1. Supplementary Online Figures

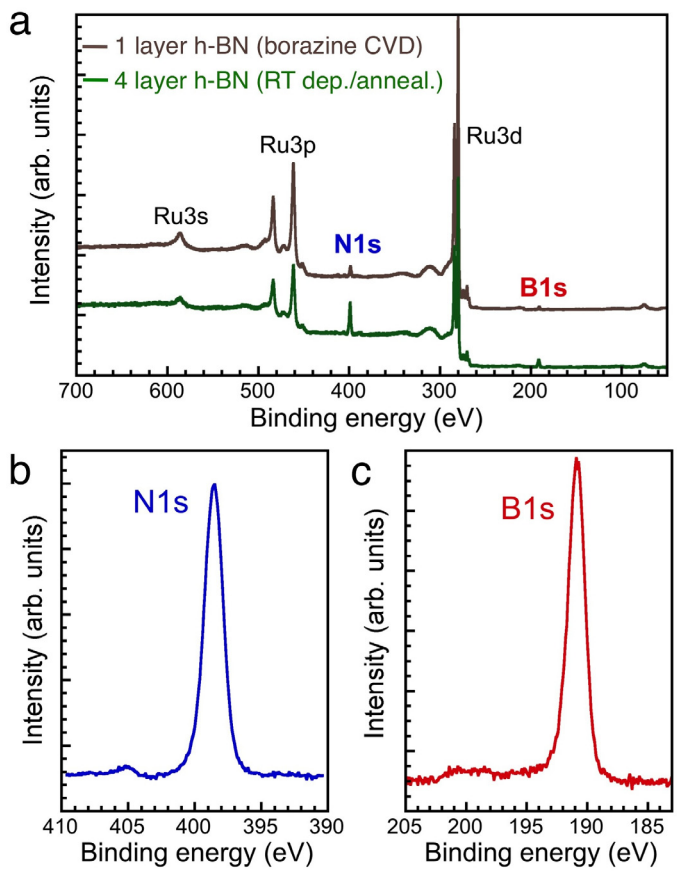

Figure S1 – XPS analysis of 1-layer and 4-layer h-BN films on Ru(0001). a) Survey XPS scans of samples grown by borazine chemical vapor deposition (CVD) [1 BN layer], and by alternating room temperature magnetron sputter deposition and 850°C annealing [4 BN layers]. **b)** N1s peak and **c)** B1S peak of the 4-layer film.

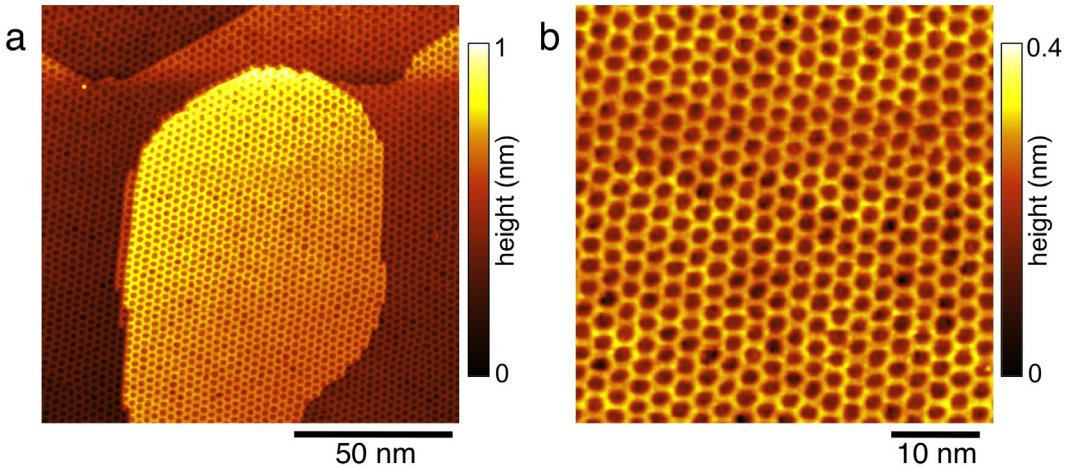

Figure S2 – STM imaging of thin BN/Ru(0001) [~1.3 atomic layers BN coverage] grown by magnetron sputtering at 850°C. a) Survey scan. **b)** High magnification image of the h-BN 'nanomesh' surface structure.

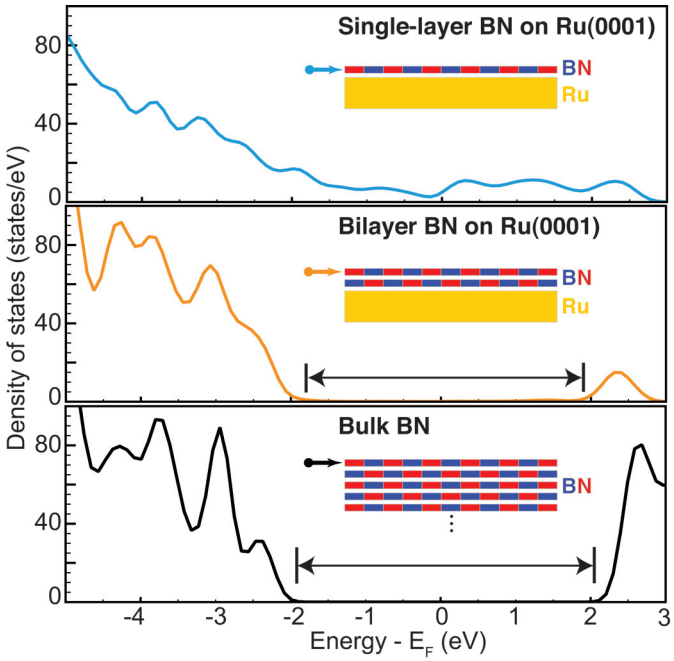

Figure S3 – Computational results on the reactivity of the surfaces of single- and bilayer h-BN on Ru(0001), and comparison with bulk h-BN. Monolayer BN/Ru(0001) shows a finite projected density of states (DOS) near the Fermi energy (E_F). At the surface of bilayer BN/Ru(0001) a large bandgap with negligible DOS opens up, comparable to the gap found for bulk BN. The low DOS near E_F indicates a low reactivity of the surface of bilayer BN. The same trend is reflected in the calculated binding energy of a B_3N_3 radical on these surfaces. Whereas B_3N_3 binds strongly on monolayer BN/Ru(0001) (binding energy 0.9 eV), the binding energy on bilayer BN/Ru(0001) is indistinguishable from that on the inert bulk BN surface (0.5 eV). For computational methods, see below.

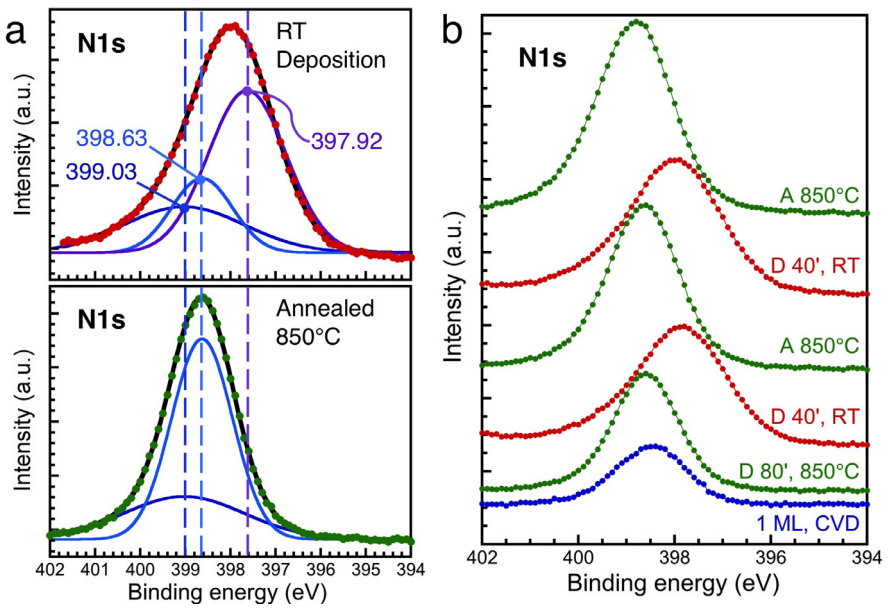

Figure S4 – Alternating room temperature BN deposition and annealing - analysis of the N1s peak shape. a) Comparison of the N1s line shape after room temperature BN growth by reactive magnetron sputtering (top), and following annealing at 850°C. **b)** N1s line shape after 1-layer borazine CVD growth of h-BN/Ru(0001), high-temperature ~2-layer growth by magnetron sputtering, and alternating room temperature deposition (D) and annealing (A).

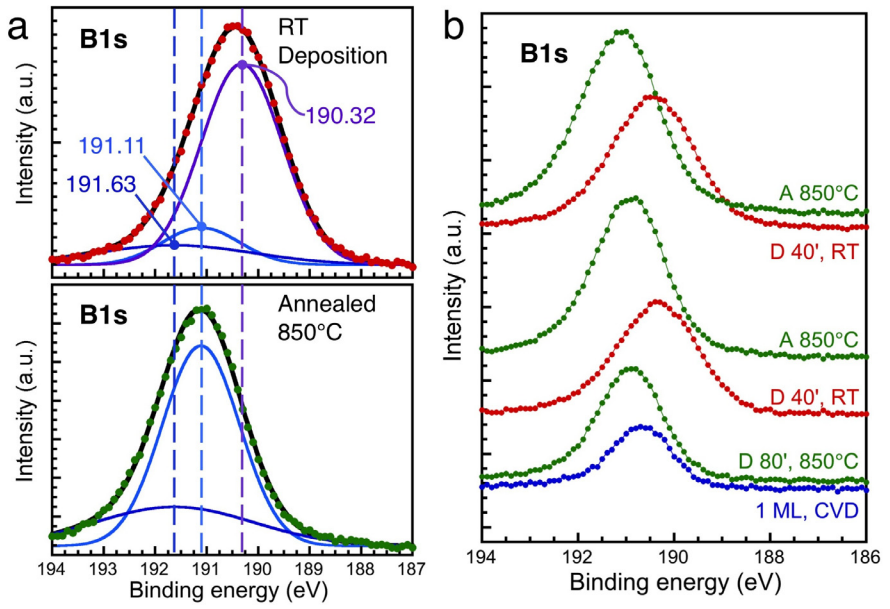

Figure S5 – Alternating room temperature BN deposition and annealing - analysis of the B1s peak shape. a) Comparison of the B1s line shape after room temperature BN growth by reactive magnetron sputtering (top), and following annealing at 850°C. **b)** N1s line shape after 1-layer borazine CVD growth of h-BN/Ru(0001), high-temperature ~2-layer growth by magnetron sputtering, and alternating room temperature deposition (D) and annealing (A).

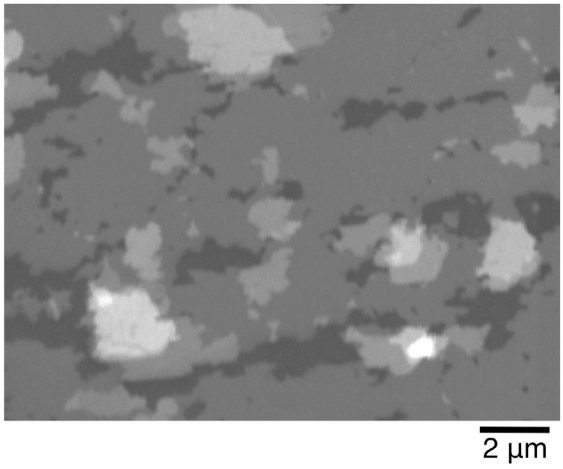

Figure S6 – UHV scanning electron microscopy image of a thicker (~ 6 layer) BN film on Ru(0001).

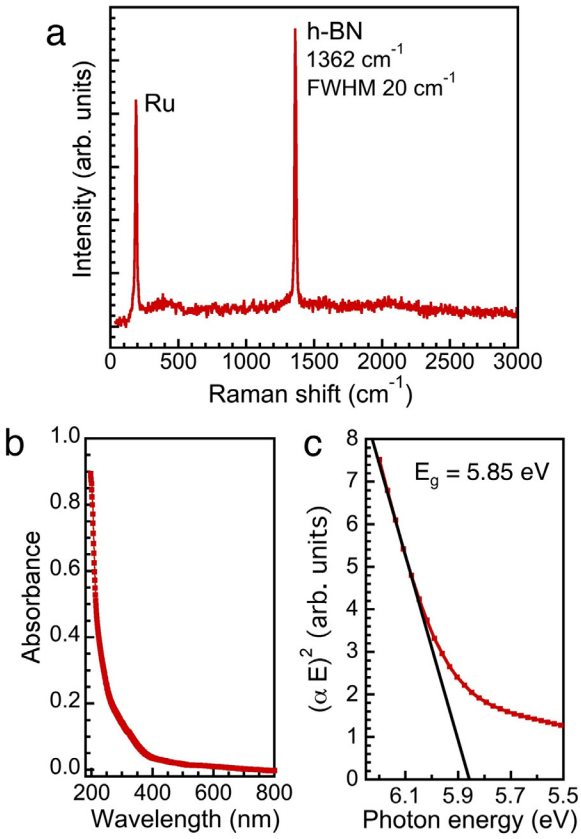

Figure S7 – Optical UV/Vis and Raman spectroscopy on few-layer BN/Ru(0001). a) Raman spectrum obtained near an edge of a BN film lifted off from the Ru substrate, showing sharp lines due to the transverse optical zone center phonon mode of Ru at ~190 cm^{-1},[1] and the E_{2g} zone center mode of h-BN at 1362 cm^{-1}. **b)** UV/Vis spectrum obtained in reflection geometry on a 10-layer h-BN film on Ru(0001). **c)** Analysis of the energy-dependent absorbance of the film, showing an optical bandgap E_g = 5.85 eV.

2. Computational Methods - Reactivity of BN surfaces

To assess the reactivity of monolayer and bilayer BN surfaces in comparison with the surface of bulk BN, calculations using density functional theory (DFT) were performed using the VASP package.[2] The projector augmented wave (PAW) method[3,4] was used to describe the electron–core interaction. The Perdew, Burke, and Ernzerhof (PBE) exchange-correlation functional[5] in the generalized gradient approximation (GGA) was used. The energy cutoff was set to 300 eV. The Brillouin zone of the supercell was sampled with a single k-point at Γ. The supercell had one or two h-BN layers on a three-layer slab of Ru with the periodicity of the full BN/Ru moiré unit cell.[6] The BN and the uppermost Ru layer were free to relax until the forces reached 50 meV $Å^{-1}$. The van der Waals interaction was taken into account using the semi-empirical correction scheme, the DFT + D approach.[7] The projected density of states (DOS) at the surface was computed for monolayer and bilayer BN on Ru(0001), and compared with the surface of bulk BN. We have also checked various binding sites for a B_3N_3 radical on the three surfaces (monolayer BN/Ru, bilayer BN/Ru, bulk BN) to model the adsorption of BN species in the reactive magnetron sputtering process. For bulk BN, the binding energy is 0.5 eV. The B_3N_3 binding energy on monolayer h-BN/Ru is substantially higher (0.9 eV), as expected due to the finite DOS near the Fermi energy. With the addition of a second BN layer, the binding of B_3N_3 at the surface of bilayer h-BN/Ru weakens and becomes indistinguishable from that on the surface of bulk BN (0.5 eV).

3. References

1. Olijnyk, H., Jephcoat, A. P. & Refson, K. On optical phonons and elasticity in the hcp transition metals Fe, Ru and Re at high pressure. *EPL (Europhysics Letters)* **53**, 504-510 (2001).
2. Kresse, G. & Hafner, J. Ab-Initio Molecular Dynamics for Liquid Metals. *Phys. Rev. B* **47**, 558 (1993).
3. Blöchl, P. E., Jepsen, O. & Andersen, O. K. Improved tetrahedron method for Brillouin-zone integrations. *Phys. Rev. B* **49**, 16223 (1994).
4. Kresse, G. & Joubert, D. From ultrasoft pseudopotentials to the projector augmented-wave method. *Phys. Rev. B* **59**, 1758-1775 (1999).
5. Perdew, J. P., Burke, K. & Ernzerhof, M. Generalized gradient approximation made simple. *Phys. Rev. Lett.* **77**, 3865-3868 (1996).

6. Wang, B. & Bocquet, M.-L. Monolayer Graphene and h-BN on Metal Substrates as Versatile Templates for Metallic Nanoclusters. *The Journal of Physical Chemistry Letters* **2**, 2341-2345 (2011).
7. Grimme, S. Semiempirical GGA-type density functional constructed with a long-range dispersion correction. *Journal of Computational Chemistry* **27**, 1787-1799 (2006).